

Nonlinear inversion of the integral equation to estimate ocean wave spectra from HF radar

Yukiharu Hisaki

Communications Research Laboratory, Okinawa Radio Observatory, Okinawa, Japan

Abstract. Since all ocean wave components contribute to the second-order scattering of a high-frequency radio wave by the sea surface, it is theoretically possible to estimate the ocean wave spectrum from first- and second-order scattering in the Doppler spectrum measured with an HF ocean radar. To extract the wave spectral information, however, it is necessary to solve a nonlinear integral equation. This paper describes in detail how to solve the nonlinear integral equation without linearization or approximation. We show that the problem of solving the nonlinear integral equation can be converted into a nonlinear optimization problem. An algorithm to find the optimal solution is described. Examples of the algorithm applied to simulated data and measured data are shown. The wave frequency spectrum can be estimated even if the Doppler spectrum is available in only a single direction. In this case, however, the solution of the two-dimensional wavenumber spectrum tends to converge to a spectrum that is symmetrical to the beam direction. Even if the wave spectrum is dominant in a single direction, the solution may give two peaks in the wavenumber spectrum. One of them is the true peak and the other is the mirror image of it with respect to the beam direction. This ambiguity can be avoided by using Doppler spectra measured in at least two different directions. Although there is still some room for improvement in the practical application of this method, it can be applied to estimate the wave directional spectrum up to a rather high frequency, or Bragg frequency.

1. Introduction

Ocean waves can be expressed by a superposition of linear fundamental waves as the first approximation. Consequently, they are usually described in terms of an ocean wave spectrum. Since wave frequency spectra can be measured rather easily, there have been many studies on wave frequency spectra and their characteristics [e.g., *Kahma*, 1992].

On the other hand, because it is difficult to measure directional spectra, there are only a few studies of two-dimensional wavenumber spectra, even though the measurement of two-dimensional wave spectra is essential in revealing the nature of wind waves. Demands for the measurement of directional spectra are not limited to scientific studies but also can be found in many marine activities such as vessel navigation and in engineering projects. Remote sensing is one technique to estimate ocean wave spectra, and a high-frequency

(HF) ocean radar has the potential to routinely measure directional spectra.

To estimate an ocean wave spectrum from HF radar data, it is necessary to solve a complicated two-dimensional nonlinear integral equation. This inversion problem has been studied by a number of researchers [e.g., *Lipa*, 1977, 1978; *Wyatt*, 1990; *Howell and Walsh*, 1993]. In these studies the linearization or approximation of the integral equation is used because of the difficulty in solving such a complicated, large-scale, nonlinear integral equation, and because previous studies aim at tractability in the estimation of a wave spectrum.

Lipa [1977, 1978] was the first to demonstrate that a directional spectrum can be estimated from a second-order echo. However, she concentrated on estimating directional information only for short saturated waves and assumed that directional properties are not dependent on wave frequencies for long unsaturated waves. However, this assumption is not generally valid both when swell components are present and when only wind waves are present [e.g., *Mitsuyasu et al.*, 1975]. *Wyatt* [1990] explicitly assumes a wave spectral form at high frequen-

Copyright 1996 by the American Geophysical Union.

Paper number 95RS02439.
0048-6604/96/95RS-02439\$08.00

cies, and the nonlinear integral equation is then modified into a linear integral equation which can be solved by the relaxation method. Her method fails when the explicitly assumed wave spectral form at high frequencies is not representative of the true wave spectrum. *Howell and Walsh* [1993] linearized the integral equation by removing one of the directional spectral product factors in the integrand as a spectral value at a certain wavenumber vector. The linearized integral equation was then modified into a matrix equation, and the matrix equation was solved by a singular value decomposition. Their approximation is valid only for much longer waves compared with radio wavelength.

Accordingly, a method without linearization or approximation needs to be developed. Full nonlinear inversion is the ultimate goal of HF ocean radar researchers [*Wyatt and Holden*, 1992]. In this paper we describe a method in detail to solve the nonlinear integral equation to estimate the ocean wave spectrum from HF radar data. To my knowledge, this is the first approach of this kind to the problem in this field. In section 2 the formulation of HF radio wave scattering by the sea surface is reviewed. In the following section the formulation of the nonlinear optimization problem is presented. An algorithm to solve this large-scale nonlinear optimization problem is proposed and summarized in section 4. Numerical examples of the estimation of directional spectra are presented in section 5 for simulated and measured Doppler spectra. The conclusions, significance of this study, and subjects for the future study are summarized in section 6.

2. Backscattering of HF Radio Waves by the Sea Surface

Sea surface waves can be expressed by superposing fundamental (linear) waves as the first approximation and by superposing bound waves as the second approximation. Bound waves are generalized Stokes-type harmonics. A bound wave component is the product of a nonlinear coupling by two fundamental wave components [e.g., *Weber and Barrick*, 1977]. Both fundamental waves and bound waves contribute to the scattering of HF radio waves.

The scattering of HF radio waves by the sea surface is caused by Bragg scattering [*Crombie*, 1955]. Figure 1 is an example of a Doppler spectrum of scattered radio waves by the sea surface at a

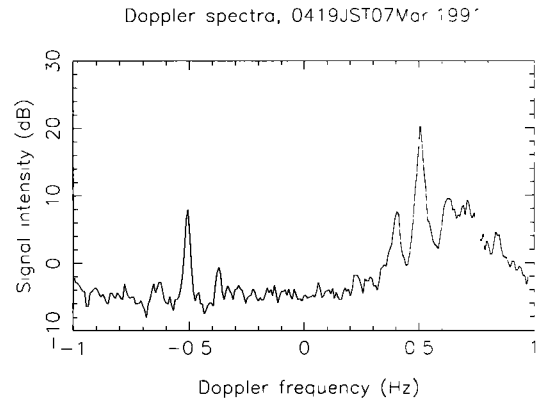


Figure 1. An example of a Doppler spectrum obtained by the HF ocean radar.

grazing incidence. There are two large peaks at about 0.5 Hz in this figure. These are called first-order scattering and are caused by the fundamental ocean wave components whose wavenumber vectors are plus or minus $2\mathbf{k}_0$. Without considering ocean currents, the Doppler frequency of the peak is called the Bragg frequency. Since the first-order scattering is caused by Bragg scattering of fundamental (linear) wave components, the Bragg frequency ω_B is obtained by the linear dispersion relation as

$$\omega_B = [2gk_0 \tanh(2k_0d)]^{1/2}, \quad (1)$$

where g is the gravitational acceleration, d is the water depth, and k_0 is the magnitude of \mathbf{k}_0 . The fundamental wave components whose wave frequency is ω_B and wave vector is plus or minus $2\mathbf{k}_0$ are termed “Bragg wave components.” There are also smaller peaks surrounding the first-order peaks in Figure 1. They are called second-order scattering. They are primarily caused by bound waves whose wavenumber vectors are plus or minus $2\mathbf{k}_0$ [*Hisaki and Tokuda*, 1995a]. All fundamental wave components contribute to the bound waves whose wavenumber vectors are plus or minus $2\mathbf{k}_0$; that is, all fundamental wave components contribute to first- or second-order scattering. Therefore it is theoretically possible to estimate a wave spectrum composed of fundamental waves from the Doppler spectrum at a single radio frequency by using first- and second-order scattering. The Doppler spectral density $P(\omega_D)$ at Doppler frequency ω_D is proportional to the radar cross section per unit frequency $\sigma(\omega_D)$; that is,

$$\begin{aligned}
P_i(\omega_D) &= A\sigma_i(\omega_D) \quad i = 1, 2, \\
P(\omega_D) &= P_1(\omega_D) + P_2(\omega_D), \\
\sigma(\omega_D) &= \sigma_1(\omega_D) + \sigma_2(\omega_D), \quad (2)
\end{aligned}$$

where $P_1(\omega_D)$ and $P_2(\omega_D)$ are the first- and second-order Doppler spectral densities and A is an unknown factor. If we normalize the frequency and wavenumber by ω_B and $2k_0$, the normalized first- and second-order radar cross sections $\sigma_{iN}(\omega_{DN}) = \omega_B \sigma_i(\omega_D)$ ($i = 1, 2$) can be written in the normalized form, as follows [e.g., *Lipa and Barrick, 1986; Holden and Wyatt, 1992; Hisaki and Tokuda, 1995a*]:

$$\sigma_{1N}(\omega_{DN}) = 4\pi S_N(-m_2 \hat{N}) \delta(\omega_{DN} - m_2), \quad (3)$$

$$\begin{aligned}
&\sigma_{2N}(\omega_{DN}) \\
&= 8\pi \int_{-\infty}^{+\infty} \int_0^{+\infty} |\Gamma_{TN}^s|^2 S_N(m_1 \mathbf{k}_{1N}) S_N(m_2 \mathbf{k}_{2N}) \\
&\quad \cdot \delta(\omega_{DN} - h_s) dp_N dq_N, \quad (4)
\end{aligned}$$

where

$$\begin{aligned}
h_s &= \coth^{1/2} d_N (m_1 k_{d1N}^{1/2} + m_2 k_{d2N}^{1/2}), \\
h_s &= m_1 \omega_{1N} + m_2 \omega_{2N} \quad (5)
\end{aligned}$$

and \hat{N} is a unit vector defined as $\hat{N} = 2\mathbf{k}_0 / (2k_0)$. Here, the normalized spatial wavenumber p_N is defined along the radar beam, q_N is perpendicular to it, and $\hat{N} = (1, 0)^T$ in the p_N - q_N plane; $\omega_{DN} = \omega_D / \omega_B$ is the normalized wave frequency, $d_N = 2k_0 d$ is the normalized water depth, and the sign (m_1, m_2) is determined from the range of the normalized Doppler frequency ω_{DN} as

$$\begin{aligned}
(m_1, m_2) &= (-1, -1) \quad \text{for } \omega_{DN} < -1 \\
(m_1, m_2) &= (1, -1) \quad \text{for } -1 < \omega_{DN} < 0 \\
(m_1, m_2) &= (-1, 1) \quad \text{for } 0 < \omega_{DN} < 1 \\
(m_1, m_2) &= (1, 1) \quad \text{for } \omega_{DN} > 1. \quad (6)
\end{aligned}$$

The subscript N denotes normalization in this manner, and details of the normalization are described by *Lipa and Barrick [1986]* and *Hisaki and Tokuda [1995a]*.

$S_N(\mathbf{k}_N)$ is the wave vector spectrum composed of fundamental waves for wavenumber vector \mathbf{k}_N .

Here, k_{iN} , k_{diN} , and ω_{iN} ($i = 1, 2$) are expressed as follows for $\boldsymbol{\kappa}_N = (p_N, q_N)$:

$$\mathbf{k}_{iN} = -\frac{1}{2} \hat{N} + (3 - 2i) \boldsymbol{\kappa}_N, \quad (7)$$

$$\mathbf{k}_{diN} = \tanh(k_{iN} d_N) \mathbf{k}_{iN}, \quad (8)$$

$$\omega_{iN} = [k_{iN} \coth(d_N) \tanh(k_{iN} d_N)]^{1/2}, \quad (9)$$

and wavenumbers $k_{iN} = |\mathbf{k}_{iN}|$ and $k_{diN} = |\mathbf{k}_{diN}|$. Equation (9) shows the linear dispersion relation and is satisfied by arbitrary fundamental wave components.

By symmetry, the integral in (4) is taken only over $p_N \geq 0$, and the inequality $k_{1N} \leq k_{2N}$ is satisfied. Γ_{TN}^s is called the coupling coefficient, and it is expressed as follows;

$$\Gamma_{TN}^s = \Gamma_{EN}^s - i\Gamma_{HN}^s \quad (10)$$

Γ_{HN}^s and Γ_{EN}^s are called the hydrodynamic and electromagnetic coupling coefficients, respectively. The former represents the effects of bound waves and the latter represents the effects of double Bragg scattering [e.g., *Hisaki and Tokuda, 1995a*]. The double Bragg scattering is due to double scattering of radio waves by a pair of fundamental ocean waves whose wavenumber vectors are written as (7). Γ_{HN}^s and Γ_{EN}^s are expressed as follows:

$$\begin{aligned}
\Gamma_{HN}^s &= \frac{1}{2} \left\{ k_{d1N} + k_{d2N} + \frac{(k_{d1N} k_{d2N} - \mathbf{k}_{1N} \cdot \mathbf{k}_{2N})}{m_1 m_2 (k_{d1N} k_{d2N})^{1/2}} \left(\frac{1 + \omega_{DN}^2}{1 - \omega_{DN}^2} \right) \right. \\
&\quad \left. - \frac{\omega_{DN} [m_1 k_{d1N}^{3/2} \operatorname{cosech}^2(k_{1N} d_N) + m_2 k_{d2N}^{3/2} \operatorname{cosech}^2(k_{2N} d_N)]}{(\tanh d_N)^{1/2} (1 - \omega_{DN}^2)} \right\}. \quad (11)
\end{aligned}$$

$$\Gamma_{EN}^s = \frac{1}{2} \left[\frac{(\mathbf{k}_{1N} \cdot \hat{N})(\mathbf{k}_{2N} \cdot \hat{N}) - 2\mathbf{k}_{1N} \cdot \mathbf{k}_{2N}}{(\mathbf{k}_{1N} \cdot \mathbf{k}_{2N})^{1/2} - \Delta/2} \right], \quad (12)$$

where Δ is the normalized surface impedance.

The expression of the first-order radar cross section (3) is modified in terms of the frequency directional spectrum $G(\omega, \theta)$ for the numerical calculation and takes the following form for an arbitrary beam direction ψ_b :

$$\sigma_{1N}(\omega_{DN}) = C_f G_N \left(1, \psi_b - \frac{m_2 + 1}{2} \pi \right) \delta(\omega_{DN} - m_2), \quad (13)$$

where $G_N(\omega_N, \theta) = (2k_0)^2 \omega_B G(\omega, \theta)$ is the normalized frequency directional spectrum, and

$$C_f = 4\pi \left[\frac{1}{k_N} \frac{\partial \omega_N}{\partial k_N} \right]_{k_N=1}. \quad (14)$$

Since the spectra are composed of fundamental waves, the relation

$$S_N(\mathbf{k}_N) = \frac{1}{k_N} \frac{\partial \omega_N}{\partial k_N} G_N(\omega_N, \theta) \quad (15)$$

is satisfied. From (9),

$$\frac{\partial \omega_N}{\partial k_N} = \frac{1}{2} [k_N \tanh(k_N d_N) \tanh(d_N)]^{-1/2} \cdot [\tanh(k_N d_N) + k_N d_N \operatorname{sech}^2(d_N)]; \quad (16)$$

therefore, (14) is modified to

$$C_f = 2\pi(1 + 2d_N \operatorname{cosech}(2d_N)). \quad (17)$$

On the other hand, (4) is modified to

$$\begin{aligned} \sigma_{2N}(\omega_{DN}) &= \int_{-\theta_L + \psi_b}^{\theta_L + \psi_b} K_I(\omega_{DN}, \theta_b) G_N(\omega_{1N}, \theta_1) G_N(\omega_{2N}, \theta_2) d\theta. \end{aligned} \quad (18)$$

where $\theta_b (= \theta - \psi_b)$ is the direction relative to the beam direction; θ_L is determined from the condition that there exists k_{EN} which satisfies $k_{EN} = k_{1N} = k_{2N}$, $h_s = 0$, and $k_{EN} > 1/2$ [Lipa and Barrick, 1986]. If

$$\omega_{DN}^2 > \frac{2}{1 + \operatorname{sech}(d_N)}, \quad (19)$$

then

$$\theta_L = \pi - \arccos\left(\frac{1}{2k_{EN}}\right), \quad (20)$$

where k_{EN} satisfies the equation

$$k_{EN} \tanh(k_{EN} d_N) = \frac{\omega_{DN}^2}{4} \tanh d_N. \quad (21)$$

Otherwise, $\theta_L = \pi$. In the examples presented in this paper $\theta_L = \pi$. To combine measured Doppler

spectra and remove the unknown factor A , (13) and (18) can be written from (2) as

$$\frac{G_N(1, \psi_b - \pi)}{G_N(1, \psi_b - \pi) + G_N(1, \psi_b)} = \frac{\int_0^{+\infty} P_{1N}(\omega_{DN}) d\omega_{DN}}{\int_{-\infty}^{+\infty} P_{1N}(\omega_{DN}) d\omega_{DN}}, \quad (22)$$

and

$$\begin{aligned} \frac{\sigma_{2N}(\omega_{DN})}{C_f [G_N(1, \psi_b - \pi) + G_N(1, \psi_b)]} &= \frac{P_{2N}(\omega_{DN})}{\int_{-\infty}^{+\infty} P_{1N}(\omega_{DN}) d\omega_{DN}}, \end{aligned} \quad (23)$$

where $P_{iN}(\omega_{DN}) = P_i(\omega_D)$ ($i = 1, 2$). The right sides of (22) and (23) are estimated from a measured Doppler spectrum. To estimate the ocean wave spectrum from HF radar, we must solve the nonlinear integral equations (18), (22), and (23).

For the numerical integration of (18), ω_{iN} and θ_i ($i = 1, 2$) are calculated for a given ω_{DN} and $\theta(1) = \theta (= \theta_b + \psi_b)$ as

$$k_{1N} = y_*^2, \quad (24)$$

$$k_{2N} = (k_{1N}^2 + 2k_{1N} \cos \theta_b + 1)^{1/2}, \quad (25)$$

$$\theta_i = \theta(i) - \frac{\pi}{2} (m_i - 1), \quad (i = 1, 2) \quad (26)$$

$$\theta(2) = -\pi + \arcsin\left(\frac{k_{1N}}{k_{2N}} \sin \theta_b\right) + \psi_b, \quad (27)$$

and $y_* = y_*(\omega_{DN}, \theta_b)$ is the solution of the equation

$$\omega_{DN} - h_s = 0, \quad (28)$$

for $y = k_{1N}^{1/2}$, where $h_s = h_s(y, \theta_b)$ is defined in (5). Wave frequencies ω_{iN} ($i = 1, 2$) are calculated from k_{iN} by (9). Wave directions $\theta(1) = \theta$, $\theta(2)$, θ_1 , and θ_2 are the respective directions of wave vectors \mathbf{k}_{1N} , \mathbf{k}_{2N} , $m_1 \mathbf{k}_{1N}$, and $m_2 \mathbf{k}_{2N}$ in (4). Equations (25) and (27) are derived from (7). Equation (28) is solved numerically using the Newton-Raphson method. The integral kernel $K_I(\omega_{DN}, \theta_b)$ is written as

$$K_1(\omega_{DN}, \theta_b) = 16\pi \left[\left| \Gamma_{TN}^s \right| 2y^3 \left| \frac{\partial y}{\partial h_s} \right| \frac{1}{k_{1N}} \frac{\partial \omega_{1N}}{\partial k_{1N}} \frac{1}{k_{2N}} \frac{\partial \omega_{2N}}{\partial k_{2N}} \right]_{y=y_*}, \quad (29)$$

and from (5), (24), and (25),

$$\frac{\partial y}{\partial h_s} = \left[m_1 \frac{\partial k_{1N}}{\partial y} \frac{\partial \omega_{1N}}{\partial k_{1N}} + m_2 \frac{\partial k_{2N}}{\partial y} \frac{\partial \omega_{2N}}{\partial k_{2N}} \right]^{-1}$$

$$\frac{\partial y}{\partial h_s} = \left[2y \left(m_1 \frac{\partial \omega_{1N}}{\partial k_{1N}} + m_2 \frac{y^2 + \cos \theta_b}{k_{2N}} \frac{\partial \omega_{2N}}{\partial k_{2N}} \right) \right]^{-1}, \quad (30)$$

where $\partial \omega_{iN}/\partial k_{iN}$ ($i = 1, 2$) is calculated from (16).

3. Formulation to the Nonlinear Optimal Problem

3.1. Fundamental Wave Components

All of the fundamental wave components are related to the Doppler spectra. However, the components in the wave spectrum that can be estimated are limited, because of the low signal-to-noise (SN) ratio and of the limitations of second-order scattering theory [Hisaki and Tokuda, 1995b] at high Doppler frequencies in high wave conditions. Therefore only the second-order peaks surrounding the first-order echoes, which are related to the energetic region of the wave spectrum, can be used for the calculation. The first step of the algorithm to estimate ocean wave spectra from HF radar data is to determine fundamental wave components from the range of Doppler frequencies in the algorithm. The relations between the Doppler frequency (ω_{DN}) and the wave component ((ω_{1N}, θ_1) or (ω_{2N}, θ_2)) are expressed in (9) and (25)–(28). Let us consider these relations. If the wave component corresponds to the (ω_{1N}, θ_1) wave component (from now on, we will refer to (ω_{1N}, θ_1) as the “ $k1$ wave” and (ω_{2N}, θ_2) as the “ $k2$ wave”), k_{1N} is obtained from the linear dispersion relation (9), and k_{2N} is calculated from

$$k_{2N} = (k_{1N}^2 + 2m_1 k_{1N} \cos \theta_b + 1)^{1/2}. \quad (31)$$

Since $k_{1N} < k_{2N}$,

$$2m_1 k_{1N} \cos \theta_b + 1 > 0 \quad (32)$$

must be satisfied. Here, the relation between (ω_N, θ) of the $k1$ wave and ω_{DN} is considered. That is to

say, we consider $m_1 k_{1N}$ instead of k_{1N} in (4); hence (31) is slightly different from (25). The θ_1 in (26) corresponds to $\theta (= \theta_b + \psi_b)$ in (31). Similarly, if the wave component is a $k2$ wave, k_{2N} is obtained from the linear dispersion relation (9) in the same manner, and k_{1N} is calculated from

$$k_{1N} = (k_{2N}^2 + 2m_2 k_{2N} \cos \theta_b + 1)^{1/2}. \quad (33)$$

In this case,

$$2m_2 k_{2N} \cos \theta_b + 1 < 0 \quad (34)$$

must be satisfied. The relation between (ω_N, θ) of the ki wave ($i = 1, 2$) and ω_{DN} can be written for deep water as follows:

for the $k1$ wave,

$$\omega_{DN} = m_1 \omega_N + m_2 [\omega_N^4 + 2m_1 \omega_N^2 \cos(\theta - \psi_b) + 1]^{1/4}, \quad (35)$$

and for the $k2$ wave,

$$\omega_{DN} = m_1 [\omega_N^4 + 2m_2 \omega_N^2 \cos(\theta - \psi_b) + 1]^{1/4} + m_2 \omega_N, \quad (36)$$

from (5), (9), (28), (31), and (33). Figure 2 shows Doppler frequency contours to wave components for $d_N = \infty$, $\psi_b = 0$, and $\omega_{DN} > 0$ as expressed by (35) and (36). The figure is symmetrical to 0° , and if $\omega_{DN} < 0$, it is symmetrical to 90° . The $k2$ wave components are confined around $(1, \pm 180^\circ)$ for ω_{DN} of about 1. Therefore the linear approximation of the integral equation may be justified, if the Doppler frequency range used in the inversion calculation is limited near the first order scattering peaks. However, the limit of the applicability of the linearization is not clear. Nonlinear inversion is especially effective when the SN ratio of the Doppler spectrum is high enough to allow us to estimate the wave spectrum up to a fairly high frequency.

3.2. Discretization of Integral Equation

We first discretize the frequency angle $(\omega_N - \theta)$ plane. It is not necessary that the discretized grid points in the $\omega_N - \theta$ plane be uniform along the frequency direction. However, the inversion is easier if $\omega_N = 1$ is included. On the other hand, the grid points along the angle direction must be uniform, and the discretized angles are expressed as

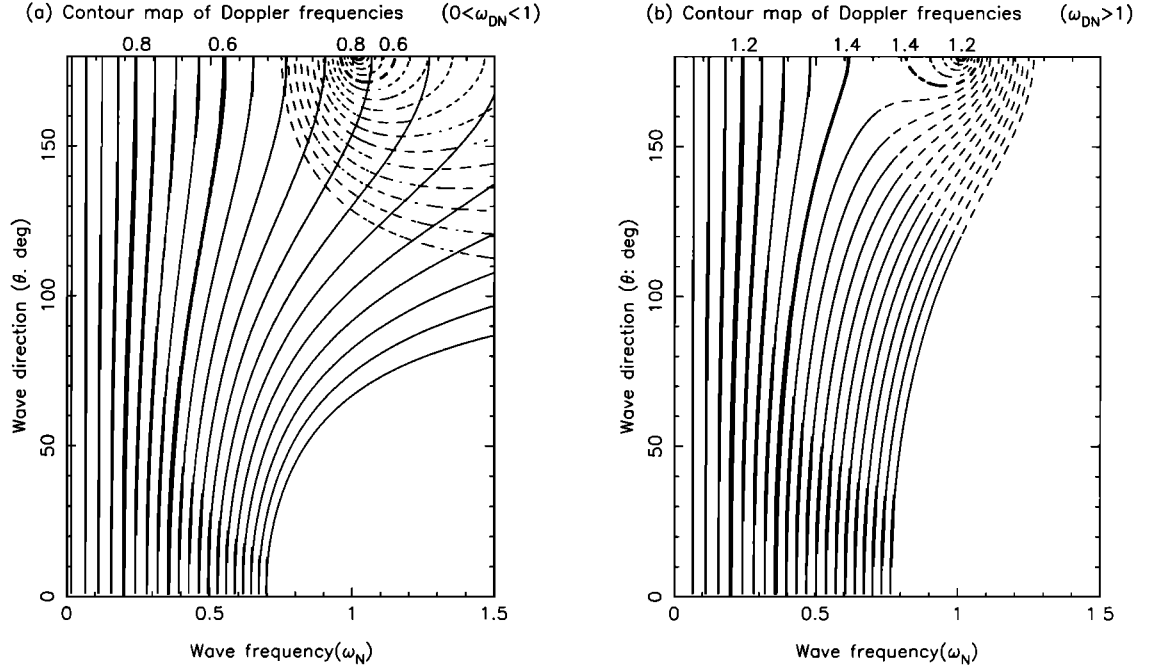


Figure 2. Doppler frequency contour map to wave components for deep water for (a) $0 < \omega_{DN} < 1$ and (b) $\omega_{DN} > 1$. Solid line, contour for the k_1 wave; dashed line, contour for the k_2 wave. The contour interval is 0.05.

$$\theta_k = -\pi + \frac{2\pi}{M} k \quad k = 0, \dots, M-1 \quad (37)$$

Each grid point is evaluated as to whether it is a wave component that corresponds to the given Doppler frequency region. If the point lies within the given Doppler frequency region, the point is numbered. Moreover, the neighboring grid points are also judged to be wave components that must be estimated. Even when a grid lies out of the Doppler frequency region, if there exists a neighboring grid that lies within the region, the outside grid is also numbered because it also constructs the discretized integral equation that is presented later (41). These numbers are termed “wave component numbers.” Figure 3, which is a magnification of Figure 2, illustrates schematically how the evaluation is done. Solid circles are the grid points of wave components to be estimated and are numbered, and the open circles are grid points which are not used in the calculation and need not be numbered. Equations (5), (9), (28), and (31) (or (33)) are used for the evaluation.

A wave spectrum $G_N(\omega_N, \theta)$ at an arbitrary point

(ω_N, θ) is expressed by the linear interpolation of spectral values at the four surrounding grid points. Let us consider numerical integration of (18) along a Doppler frequency contour in the ω_N - θ plane for the k_i wave ($i = 1, 2$). Figure 4, which is also a

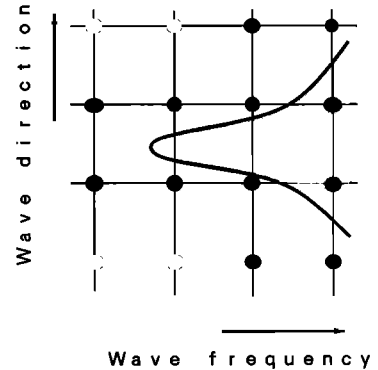


Figure 3. Schematic diagram for the determining whether a wave component is a k_1 wave or a k_2 wave. The shaded area is the region of the Doppler frequency range for the calculation. A thick curve is the boundary, and it corresponds to the upper (or lower) Doppler frequency contour.

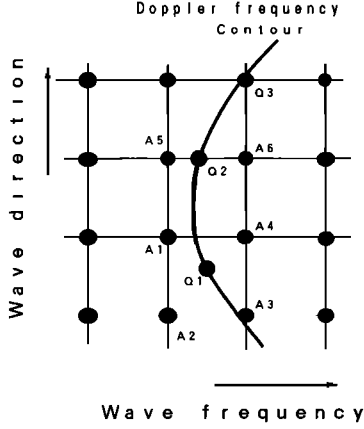


Figure 4. Schematic illustration of the interpolation of spectral values at quadrature points for the numerical integration of (18).

magnification of Figure 2, illustrates schematically the interpolation of spectral values at quadrature points for the numerical integration of (18). The spectral value at a quadrature point which is on a Doppler frequency contour is expressed by the interpolation of spectral values at the four (or two) surrounding grid points. For example, for quadrature point Q1, the spectral value at the point is interpolated by the spectral values at the four grid points A1–A4. On the other hand, if a quadrature point is on a grid line, as Q2 is, the spectral value at the point is expressed by the spectral values at the two grid points A5 and A6. If a quadrature point is on a grid point, as Q3 is, it is not necessary to interpolate the spectral value at that point. In this interpolation, (22) is discretized in the following form:

$$\frac{B_1}{B_1 + B_2} = \frac{\int_0^{+\infty} P_{1N}(\omega_{DN}) d\omega_{DN}}{\int_{-\infty}^{+\infty} P_{1N}(\omega_{DN}) d\omega_{DN}}, \quad (38)$$

where B_n ($n = 1, 2$) indicates the interpolated spectral values for the Bragg wave components, and $n = 1$ denotes the Bragg wave component for $\theta_b = -180^\circ$ (or $\theta = -\pi + \psi_b$), and $n = 2$ denotes that for $\theta_b = 0^\circ$ (or $\theta = \psi_b$). The interpolated spectral values for Bragg wave components B_n are written as

$$B_n = \sum_{p=1}^{N_B} w_B(jB(n, p)) x_{jB(n, p)} \quad n = 1, 2, \quad (39)$$

where N_B indicates the number of wave components used to interpolate the spectral value of Bragg wave components. N_B takes the value 1, 2, or 4 depending on where the point (ω_N, θ) is located. The point for the Bragg wave component in the ω_N - θ plane is $(1, -\pi + \psi_b)$ or $(1, \psi_b)$, and if the point is located on a discretized grid point, $N_B = 1$. In this case it is not necessary to interpolate the spectral value for the Bragg wave component by spectral values at surrounding grid points. If the point is located on a grid line, $N_B = 2$. Here, $jB(n, p)$ is the wave component number of the Bragg wave component (for $N_B = 1$) or of neighboring grids to the Bragg wave component ($N_B = 2, 4$), $x_{jB(n, p)}$ is a spectral value for wave component number $jB(n, p)$, and $w_B(jB(n, p))$ is a weight for the linear interpolation and satisfies

$$\sum_{p=1}^{N_B} w_B(jB(n, p)) = 1. \quad (40)$$

On the other hand, (23) is discretized in the following form for $\theta_L = \pi$:

$$\frac{2\pi \sum_{k=0}^{M-1} [K_l(\omega_{DN}, \theta_{bk}) R_1 R_2]}{M(B_1 + B_2) C_f} = \frac{P_{2N}(\omega_{DN})}{\int_{-\infty}^{+\infty} P_{1N}(\omega_{DN}) d\omega_{DN}}, \quad (41)$$

where R_i ($i = 1, 2$) indicates interpolated spectral values for the ki wave at a quadrature point which is on a Doppler frequency contour in the ω_N - θ plane, and

$$\theta_{bk} = \theta_k - \psi_b. \quad (42)$$

The interpolated spectral values R_i are written as

$$R_i = \sum_{p=1}^{2i} w(j(i, k, p)) x_{j(i, k, p)} \quad i = 1, 2, \quad (43)$$

where $j(i, k, p)$ is the wave component number of the four (or two) surrounding grid points in the ω_N - θ plane for the ki wave ($i = 1, 2$), $x_{j(i, k, p)}$ is the spectral value for the $j(i, k, p)$ wave component number, and

$w(j(i, k, p))$ is a weight of the linear interpolation by spectral values at the grid points, which satisfies

$$\sum_{p=1}^{2i} w(j(i, k, p)) = 1 \quad i = 1, 2. \quad (44)$$

The number of spectral values used for the interpolation is $2i$ for the ki wave ($i = 1, 2$). The difference between the integral variable θ in (18) and θ_1 which is the direction of the $k1$ wave is 0 or π (see (26)). Therefore, if M is an even number so that there exists k which satisfy $\theta_k = 0$, and if we choose quadrature points for the numerical integration of (18) so that the points are on discretized grid lines parallel to the ω_N axis, the points (ω_{1N}, θ_1) are also on grid lines. Hence the number of spectral values used for the interpolation is 2 for the $k1$ wave. On the other hand, the relation between θ and θ_2 , which is the direction of the $k2$ wave, is nonlinear (see (26) and (27)). Therefore the points for the $k2$ wave (ω_{2N}, θ_2) are not on discretized grid points or lines in general. Hence the number of spectral values used for the interpolation is 4 for the $k2$ wave. Equations (38) and (41) are the discretized forms of (22) and (23), respectively, and the equations must be solved to estimate the ocean wave spectrum from HF radar data.

The calculation of the left sides of (38) and (41) are as follows. First, $jB(n, p)$ and $w_B(jB(n, p))$ are determined. Second, (ω_{1N}, θ_1) , (ω_{2N}, θ_2) , and $K_l(\omega_{DN}, \theta_{bk})$ are calculated by (9), (24)–(28), and (29) for each quadrature point $(\omega_{DN}, \theta_{bk})$. Third, two (or four) neighboring grid points in the ω_N - θ plane are determined. Finally, the wave component numbers $j_B(n, p)$ and $j(i, k, p)$ and weights $w_B(j_B(n, p))$ and $w(j(i, k, p))$ are obtained.

Equations (38) and (41) are formally written in the form of

$$\mathbf{F}_l(\mathbf{x}) = \mathbf{e}_l, \quad (45)$$

where $\mathbf{F}_l = (F_1, \dots, F_{LL})^T$ is a discretized form of (38) and (41), $\mathbf{x} = (x_1, \dots, x_{NN})^T$ is the wave spectrum to be estimated, and $\mathbf{e}_l = (e_1, \dots, e_{LL})^T$ is the error vector.

3.3. Linear and Nonlinear Constraints for the Ill-Posed Problem

Solutions to (45) are generally unstable. Therefore some constraints for solutions are needed. The additional constraints used in this paper are as follows:

Constraint 1 (C1). $F_i(\mathbf{x}) = \lambda_3 x_l = 0$. Spectral values at $\omega_N \approx 0$ are close to zero, and l denotes the wave component numbers which are closest to zero frequency. The wave components closest to zero frequency are constrained.

Constraint 2 (C2). $F_i(\mathbf{x}) = \lambda_{4(5)}(s_1 x_l - x_m + s_2 x_n) = 0 (s_1 + s_2 = 1)$. Solutions change “smoothly” with frequency (or angle) for the $k1$ wave. Here, (l, m, n) denotes the frequency (or angle) neighboring wave component numbers. The “smooth change” along the frequency direction in the ω_N - θ plane is for $\omega_{F1} \leq \omega_N \leq \omega_{F2}$ (for angles, $\omega_{A1} \leq \omega_N \leq \omega_{A2}$), and s_1 and s_2 are determined by the grid interval of the discretization.

Constraint 3 (C3). $F_i(\mathbf{x}) = \lambda_{6(7)}(r_i x_l - x_m) = 0$. Solutions change “continuously” with frequency (or angle) for the $k1$ wave. The frequency regions for “continuous change” along the frequency direction are $\omega_N < \omega_{F1}$ or $\omega_N > \omega_{F2}$ (for angles, $\omega_N < \omega_{A1}$ or $\omega_N > \omega_{A2}$); r_i is determined by l and m . In this calculation, r_i is set as proportional to ω_N^{-5} for “continuous change” constraints along the frequency direction at $\omega_N > \omega_{F2}$. Otherwise, $r_i = 1$.

Constraint 4 (C4). $F_i(\mathbf{x}) = \lambda_{8(9)}(r_i x_l - x_m)/(r_i x_l + x_m) = 0$. As for (C3), but for the $k2$ wave.

Constraint 5 (C5). $F_i(\mathbf{x}) = \lambda_{10}(x_l/(x_l + x_m) - t_i) = 0$. The ratio of the $k2$ wave spectra whose angular difference is 180° is close to the ratio of the first-order echoes. Here, (l, m) denotes the 180° different $k2$ wave component numbers (l is closer to $\theta_b = -180^\circ$), and t_i is defined as

$$t_i = \frac{G_N(1, \theta_l)}{G_N(1, \theta_l) + G_N(1, \theta_l + \pi)}, \quad (46)$$

where θ_l is the angle for the l th wave component number. Here, t_i is calculated from the first-order echos with the assumed directional model. For example, if the $\cos^{2s}(\theta/2)$ directional form is assumed, and s and the mean wave direction θ_0 are estimated from the first-order echoes, t_i is written as

$$t_i = \frac{\cos^{2s}[(\theta_l - \theta_0)/2]}{\cos^{2s}[(\theta_l - \theta_0)/2] + \sin^{2s}[(\theta_l - \theta_0)/2]}.$$

Constraint 6 (C6). $F_i(\mathbf{x}) = \lambda_{11}(s_1 x_l - x_m + s_2 x_n) = 0 (s_1 + s_2 = 1)$. Solutions change “smoothly” with frequency (or angle) between the $k1$ wave and the $k2$ wave for the frequency direction in the ω_N - θ plane. In this calculation, four wave components

(two groups) at $\theta_b \approx -180^\circ$ and $\theta_b \approx 0^\circ$ are selected to construct this relation; therefore four constraints are added per beam direction.

Here λ_1 and λ_2 are the weights for (38) and (41), respectively. These constraints are not always ideal. There is room to improve them. The Lagrange multiplier λ_i is set arbitrarily here. The method of deciding the best parameters is a subject for future study. The nonlinear forms such as (C4) and (C5) are chosen to avoid a physically meaningless convergence to zero which also satisfies the "continuous change condition." Constraints (45) and (C1)–(C6) can be written as

$$\mathbf{F}(\mathbf{x}) = \mathbf{e}, \quad (47)$$

where $\mathbf{F} = (F_1, \dots, F_{LL}, \dots, F_{MM})^T$ ($MM > LL$), and $\mathbf{e} = (e_1, \dots, e_{LL}, \dots, e_{MM})^T$. Therefore the problem of solving the nonlinear integral equation results in a nonlinear optimization problem to find \mathbf{x} that minimizes the objective function $U(\mathbf{x})$ defined as

$$U(\mathbf{x}) = \frac{1}{2} \sum_{i=1}^{MM} (F_i(\mathbf{x}))^2 \quad (48)$$

subject to $x_j \geq 0$ ($j = 1, \dots, NN$). The concept of this method is the same as the regularization method for solving a linear Fredholm-type integral equation of the first kind [Twomey, 1963].

4. Algorithm for the Nonlinear Inversion

4.1. Algorithm for the Nonlinear Optimization Problem

The minimization of $U(\mathbf{x})$ is solved numerically, and the algorithm is expressed in general as follows:

$$\mathbf{d}_l = -\mathbf{H}_l \nabla U = -\mathbf{H}_l \mathbf{J}_F^T \mathbf{F}, \quad (49)$$

$$\mathbf{x}^{(l+1)} = \mathbf{x}^{(l)} + \alpha_l \mathbf{d}_l, \quad (50)$$

where l indicates the step number, α_l is a positive constant which is adjusted in such a way that $U(\mathbf{x}^{(l+1)}) < U(\mathbf{x}^{(l)})$. Here, $\mathbf{x}^{(l)} = (x_1^{(l)}, \dots, x_n^{(l)})^T$ is \mathbf{x} for l th step. The \mathbf{J}_F is the Jacobian matrix defined as

$$J_{Fij} = \frac{\partial F_i}{\partial x_j^{(l)}} \quad i = 1, \dots, MM \quad j = 1, \dots, NN. \quad (51)$$

\mathbf{H}_l is a positive definite matrix. It can be expressed in several different ways depending on the method used. A few well-known examples are as follows:

Steepest descent method

$$\mathbf{H}_l = I, \quad (52)$$

Gauss-Newton method

$$\mathbf{H}_l = (\mathbf{J}_F^T \mathbf{J}_F)^{-1}, \quad (53)$$

Marquart method

$$\mathbf{H}_l = (\mathbf{J}_F^T \mathbf{J}_F + \lambda_{Mq} I)^{-1}, \quad (54)$$

where $\lambda_{Mq} (> 0)$ is called Marquart's parameter. Although these algorithms were originally developed for an unconstrained optimization problem, they are still applicable here. Since we would like to estimate two-dimensional wave spectra, the scale of the optimization problem is large, that is, NN is large compared with computer memory capacity. In a large-scale optimization problem it may not be possible to compute and store the positive definite matrix \mathbf{H}_l used in the Gauss-Newton or Marquart method because of its size. One way to avoid such a storage problem is to choose the matrix as follows:

$$\mathbf{H}_l = [\text{diag}(\mathbf{J}_F^T \mathbf{J}_F)]^{-1} \quad (55)$$

or

$$\mathbf{H}_l = [\text{diag}(\mathbf{J}_F^T \mathbf{J}_F) + I]^{-1}. \quad (56)$$

The updating direction \mathbf{d}_l is written as

$$\mathbf{d}_l = (d_1, \dots, d_{NN})^T \quad (57)$$

where

$$d_j = \sum_{i=1}^{MM} F_i \frac{\partial F_i}{\partial x_j^{(l)}} \bigg/ \sum_{i=1}^{MM} \left(\frac{\partial F_i}{\partial x_j^{(l)}} \right)^2 \quad j = 1, \dots, NN \quad (58)$$

if (55) is adopted. Here, \mathbf{J}_{Fij} are calculated from (38), (39), (41), (43), and (C1)–(C5).

In this method, the computer memory needed can be substantially reduced. Since the computing time needed by this method is much shorter than that needed by the Marquart method for each step, the convergence to the solution is faster than with the Marquart method, even though the number of steps

is larger. Conjugate gradient methods, such as the Fletcher-Reeves, Polak-Ribière algorithm [Shanno, 1978], do not show good convergence in this problem. The solutions are constrained as $x_j \geq 0$ ($j = 1, \dots, NN$). If a negative value of x_j is estimated in the process, it is replaced by a positive value which is very close to zero. This replacement is equivalent to a slight modification of \mathbf{H}_l . However, the modified \mathbf{H}_l is still positive definite, and \mathbf{H}_l is switched back and forth between (55) and (56) if the convergence speed is slow.

4.2. Summary of Nonlinear Inversion

The nonlinear inversion algorithm is summarized as follows:

1. Set parameters such as d_N , ω_{DN} for the calculation (Doppler frequency range) ω_{Fi} , ω_{Ai} ($i = 1, 2$), and the resolution of ocean wave frequency and wave direction (or M) and the Doppler frequency. LL is determined here.

2. For each grid point in the ω_N - θ plane, judge whether the point lies within the given Doppler frequency region and number the point if it is in the region. NN is determined here.

3. For each Doppler frequency, search groups of wave component numbers ($jB(n, p)$ and $j(i, k, p)$) that correspond to each term of the discretized integral equations (38) and (41) and calculate the weighting functions $w_B(jB(n, p))$, $w(j(i, k, p))$ and the kernel $K_l(\omega_{DN}, \theta_{bk})$.

4. Search groups of wave component numbers (l, m, n) that correspond to additional conditions (C1)–(C6), and obtain r_i , s_1 , and s_2 . MM is determined here.

5. Provide an initial guess for \mathbf{x} and set the remaining parameters, such as $\lambda_1, \dots, \lambda_{11}$ and t_i .

6. Calculate $U(\mathbf{x})$, $\nabla U(\mathbf{x})$, and \mathbf{d}_l .

7. Update \mathbf{x} according to (48) and (50).

8. If the convergence criteria are not met, repeat from step (6).

Convergence is judged by monitoring $\|\nabla U\|$ or $(\sum_{i=1}^{LL} F_i^2)/2$. In this algorithm, the computation by step (4) is taken beforehand, and the output data are stored in a file.

5. Numerical Examples of the Inversion

5.1. Simulation of the Single-Beam Case

Simulations are carried out to test the validity of the nonlinear inversion algorithm. In this simulation the model spectrum is assumed to be the true solution. We calculate the Doppler spectrum by the

method of *Lipa and Barrick* [1982] and then retrieve the wave spectrum from the calculated Doppler spectrum. The calculated second-order Doppler spectrum by *Lipa and Barrick's* [1982] method is not exactly equal to the result of computation by (41), that is, $\mathbf{e}_l \neq \mathbf{0}$, because of the linear interpolations of spectral values in (41). Figures 5 and 6 are examples of the calculation for a single-beam case. The assumed ocean wave spectrum has the Pierson-Moskowitz form, where the peak wave period is 10 s, the peak wave direction relative to the beam direction for each wave frequency is not dependent on the wave frequency, and its value is 60° . The directional distribution has a $\cos^{2s}(\theta/2)$ form, where the s value obeys Mitsuyasu's formula [*Mitsuyasu et al.*, 1975]. Initial guesses are similar to the Pierson-Moskowitz form, but are proportional to ω_N^{-4} at high frequencies. The initial peak period is 7.5 s, the wave direction is 65° , and $s = 0.5$. The initial peak period can be estimated more accurately by the method of *Forget et al.* [1981]. The initial wave direction can be estimated from the first-order echoes. Since there is an ambiguity in the signs of wave direction relative to the beam direction, however, other information is necessary in the single-beam direction case. The radar frequency is 24.515 MHz; it is the frequency of our radar, and the Bragg frequency is 0.505 Hz for deep water [*Hisaki and Tokuda*, 1995b]. The parameters are set as $d_N = \infty$, $\omega_{F1} = 0$, $\omega_{F2} = 0.4$, $\omega_{A1} = \omega_{A2} = 0$, $\lambda_1 = \lambda_2 = \lambda_3 = 10$, $\lambda_4 = \lambda_5 = \lambda_7 = \lambda_9 = 0.1$, $\lambda_6 = \lambda_8 = \lambda_{10} = 5$, and $\lambda_{11} = 1$; the frequency resolution is 0.02 (in normalized form), and the angular resolution is 15° ($M = 24$) in this example. The Doppler frequency resolution is 0.02 (in normalized form) and the Doppler frequency range for the calculation is $0.66 \leq |\omega_{DN}| \leq 0.88$ and $1.14 \leq |\omega_{DN}| \leq 1.36$. The beam direction ψ_b is 0° .

The retrieved frequency spectrum agrees well with the original true frequency spectrum in this example (Figure 5). Naturally, the calculated second-order Doppler spectrum from the retrieved wave spectrum also agrees with that from the original wave spectrum. This result shows that the frequency spectrum can be estimated from data taken only in a single-beam direction. Figure 6 shows the comparison of the true and retrieved wave directional spectra. The spectral peak at $(\omega_N, \theta) = (0.2, 60^\circ)$ is evident in both true and retrieved wave directional spectra. There is, however, another spectral peak at $(\omega_N, \theta) = (0.2, -60^\circ)$

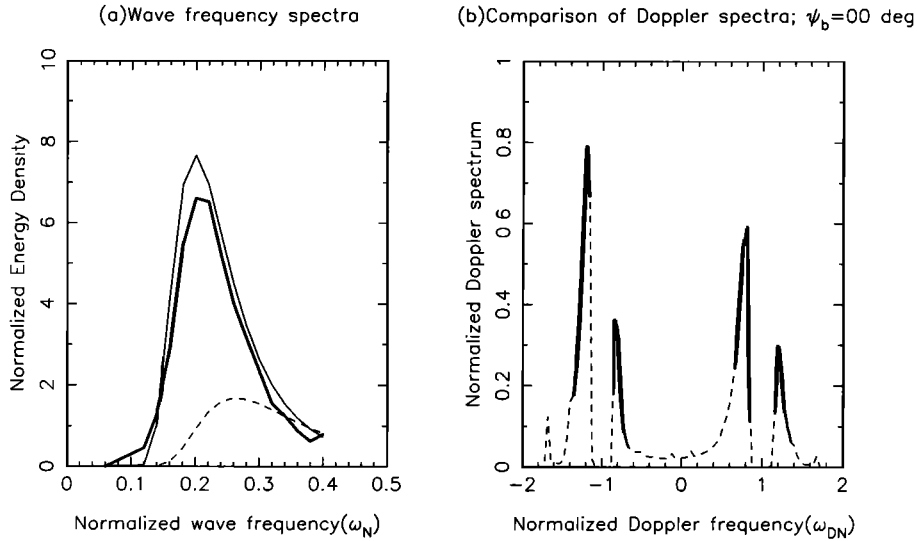


Figure 5. An example of inversion for simulated data in the single-beam case. (a) Comparison between true and retrieved frequency spectra (thin line, true solution; thick line, retrieved solution; dashed line, initial guess). (b) Comparison between true (simulated; dashed line) and retrieved (thick line) second-order Doppler spectra.

in the retrieved wave directional spectrum. The cause of this peak is due to the ambiguity in the signs of wave direction relative to the beam direction. Doppler spectra are the same for ocean wave fields whose configurations are symmetrical to the beam direction. Therefore the solutions by this

algorithm tend to converge to a solution that is symmetrical with respect to the beam direction.

5.2. Simulation for the Multiple-Beam Case

One way to avoid ambiguity is to use multiple-beam directional data. Multiple-beam directional

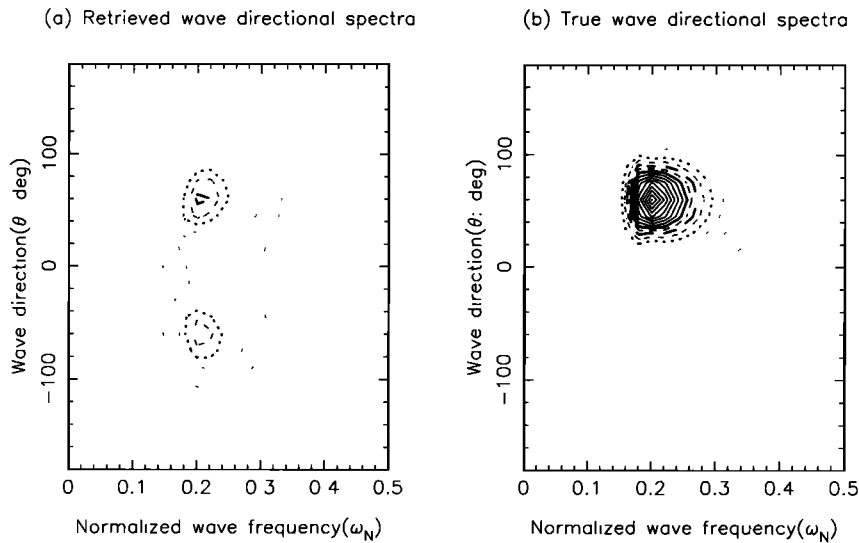


Figure 6. Comparison of wave directional spectra as in the single-beam case. (a) Retrieved directional spectra and (b) true directional spectra. Thick dotted line, 2; thick dashed line, 3; thick solid line, 4. The contour interval is 0.5.

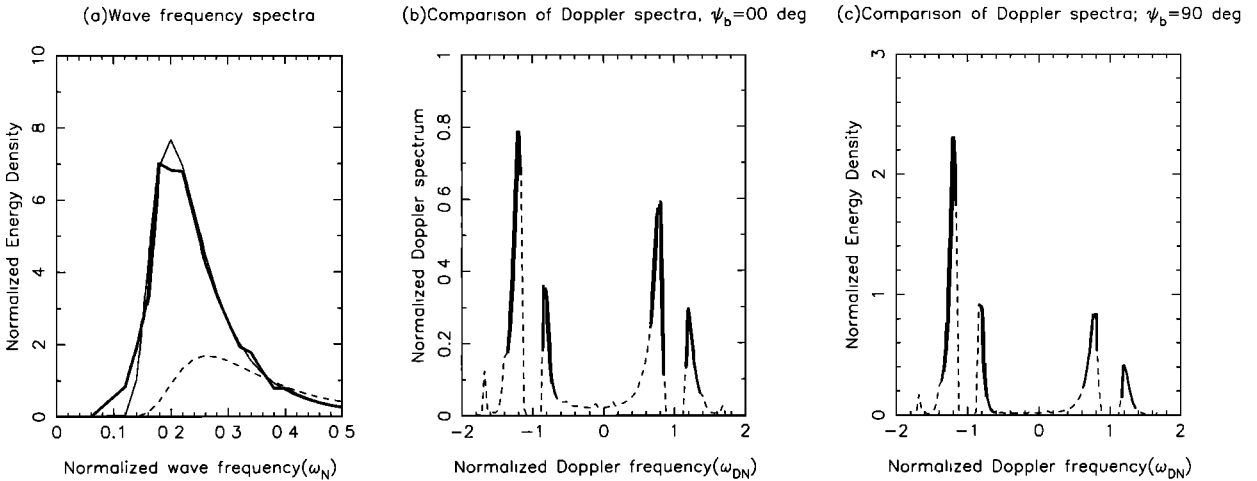


Figure 7. An example of inversion for simulated data in the dual-beam case (crossing angle is 90°). (a) Comparison between true and retrieved frequency spectra (thin line, true solution; thick line, retrieved solution; dashed line, initial guess). (b) Comparison between true (simulated; dashed line) and retrieved (thick line) second-order Doppler spectra for beam direction $\psi_b = 0^\circ$. (c) As in Figure 7b for beam direction $\psi_b = 90^\circ$.

data can be obtained by multiple radar systems or by changing beam directions assuming statistical homogeneity and stationarity of ocean waves. Figures 7 and 8 are examples of the calculations for a dual-beam directional case. The crossing angle of the two beam directions is 90° , that is, $\psi_b = 0^\circ$ and $\psi_b = 90^\circ$. The parameters are the same as for the

single-beam case, and the Doppler frequency range for the calculation for $\psi_b = 90^\circ$ is $0.62 \leq |\omega_{DN}| \leq 0.84$ and $1.14 \leq |\omega_{DN}| \leq 1.36$. The true and initial wave spectra are the same as in the previous example for the single-beam case. As can be seen, the retrieved frequency spectrum agrees well with the true spectrum. Moreover, the true and retrieved

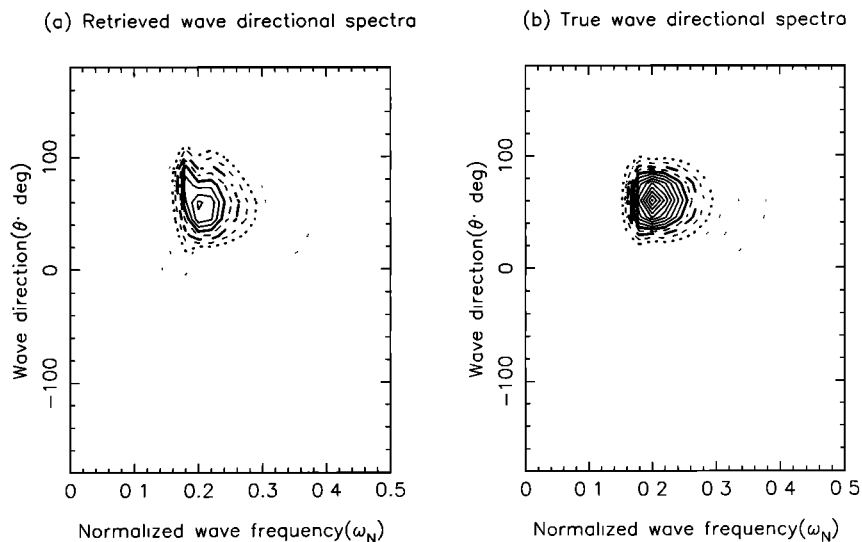


Figure 8. Comparison of wave directional spectra as in the dual-beam case. (a) Retrieved directional spectra and (b) true directional spectra. Thick dotted line, 2; thick dashed line, 3; thick solid line, 4. The contour interval is 0.5.

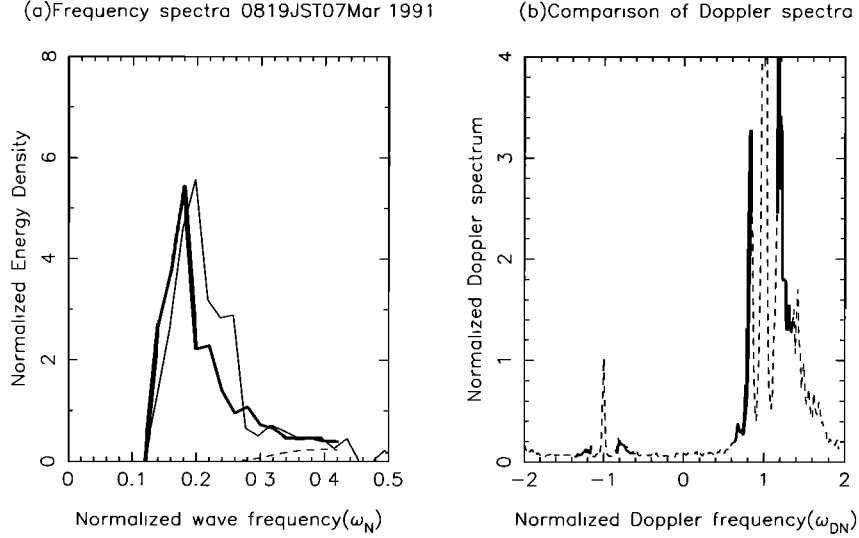


Figure 9. An example of inversion for measured Doppler spectra in the single-beam case. (a) Comparison between true and retrieved frequency spectra (thin line, true solution; thick line, retrieved solution; dashed line, initial guess). (b) Comparison between true (measured; dashed line) and retrieved (thick line) second-order Doppler spectra.

second-order Doppler spectra show a good agreement (Figure 7). There is no spectral peak at $(\omega_N, \theta) = (0.2, -60^\circ)$ in the retrieved wave in Figure 8. This shows that by using multiple-beam directional data, convergence to a spurious solution whose directional distribution is symmetrical to the beam direction can be avoided. However, we cannot in general determine the universal optimal crossing angle for a dual-beam direction case, since the optimal crossing angle depends upon the wave direction. For example, if the wave directional properties are symmetrical with respect to the beam direction, it is not necessary to use dual-beam directional data. In this case a crossing angle close to zero degrees is the optimal crossing angle.

5.3. An Example of Retrieval From Measured Doppler Spectra

The nonlinear inversion technique is applied to Doppler spectra measured in the Yura experiment. The experiment was undertaken in March 1991. The details of the experiment are described by *Hisaki and Tokuda* [1995b]. Since the accuracy of the measured directional spectra are poor, we compare only the frequency spectra. Therefore we use single-beam directional data. Figure 9 is an example of the comparison. The initial guess is the Pierson-Moskowitz form, the directional distribution is the $\cos^{2s}(\theta/2)$ form, and the wave direction and s value

are estimated from the first-order echoes [*Hisaki and Tokuda*, 1995b]. The parameters are set as $d = 100$ m, $\omega_{F1} = 0.15$, $\omega_{F2} = 0.3$, $\omega_{A1} = \omega_{A2} = 0$, $\lambda_1 = \lambda_2 = \lambda_3 = 10$, $\lambda_4 = \lambda_5 = 0.05$, $\lambda_6 = \lambda_7 = \lambda_8 = \lambda_9 = \lambda_{10} = \lambda_{11} = 1$, and $M = 20$; the Doppler frequency resolution is $\pi/(64\omega_B)$ in normalized form.

The estimated frequency spectrum agrees well with the frequency spectrum measured with a buoy. The second-order Doppler spectrum measured by radar and the second-order Doppler spectrum retrieved from the estimated wave spectrum also show agreement. However, the closeness between the measured and retrieved wave spectra depends on the initial parameters to some extent. The determination of the parameters such as the Lagrange multipliers is a subject for future study.

6. Conclusions

A nonlinear inversion method of the integral equation for estimating a wave spectrum has been developed. The integral equation is modified to a discretized form, and the constraints are added to obtain a stable solution. These overdetermined equations are solved as a nonlinear optimization problem. A simple but fast algorithm is proposed to solve the large-scale nonlinear optimization problem. The simulation results show that the frequency

spectrum can be estimated from a single-beam directional Doppler spectrum. On the other hand, the estimated directional spectrum tends to be symmetrical to the beam direction. Multiple-beam directional data should be used in order to estimate the wave directional spectrum. This method can be applied not only to simulated data but also to measured Doppler spectral data with a finite SN ratio. However, there are still some issues that must be resolved before this method can be used in practice:

1. Comparison of directional spectra with in situ measurement. We need to verify the validity of this method and find under which oceanic conditions it is applicable.

2. Optimization of parameters such as the Lagrange multipliers λ_i ($i = 1, \dots, 11$), ω_{Ai} , ω_{Fi} , ($i = 1, 2$), etc. The solution of the nonlinear optimization problem shows dependence on these parameters. Therefore we must determine the optimal values of those parameters or develop a method of automatically optimizing the parameters. However, the nonlinear equation to extract the wave spectrum from the Doppler spectrum may contain many parameters that cannot be determined from the data. That is to say, there are fewer equations for discretized integral equations (38) and (41) than the number of unknowns. Consequently, the dependence of the solution on the choice of the parameters may be inevitable in the cases presented in this paper. To determine the parameters from the measured data, we need to increase the number of independent measurements of the same area of the sea under different conditions. One possible solution to this problem is to use multiple radar systems or to measure the Doppler spectrum in several directions assuming stationary and homogeneous sea waves.

3. Elimination of noise in Doppler spectra. Since the second-order scattering signal is very small during calm sea conditions, it is difficult to estimate the wave spectrum of a calm sea. One method for avoiding this difficulty is to use several frequencies and select the frequency that gives the best SN ratio. This method, however, is not feasible in Japan because of the very limited allocation of radio frequencies for radar use. A method of reducing noise should be developed.

4. Development of a faster algorithm. The proposed algorithm is simpler and faster than the Marquart method or the conjugate gradient method.

However, it takes about 10 min to process a typical example presented in this paper with a SPARC station ELC. A faster algorithm should be developed.

Although nonlinear inversion may not be as effective when the Doppler frequency range for the calculation is limited because of a low SN ratio of the measured Doppler spectrum, the algorithm presented here can contribute to the development of a new method for estimating the wave spectrum. Although linear and nonlinear inversion are not compared in this paper, they deserve future study. The effectiveness of the nonlinear inversion will be presented in the future, because the method can be easily extended to apply to multiple-frequency or multiple-beam radar systems. Furthermore, the ranges of Doppler frequencies used in the calculation will be increased as computer capabilities improve and noise is reduced. Therefore with radar systems with improved SN ratios, HF ocean radar has the potential to become a powerful tool for estimating wave directional spectra, including higher frequencies, by making use of multiple-frequency radar systems and multiple-beam directional Doppler spectra combining multiple radar systems and changing beam directions. In this case we can demonstrate the effectiveness of nonlinear inversion.

Acknowledgments. I thank T. Iguchi, Communications Research Laboratory, for his helpful comments on the manuscript.

References

- Crombie, D. D., Doppler spectrum of sea echo at 13.56 mc./s, *Nature*, 175, 681–682, 1955.
- Forget, P., P. Broche, J. C. Maistre, and A. Fontanel, Sea state frequency features observed by ground wave HF Doppler radar, *Radio Sci.*, 16, 917–925, 1981.
- Hisaki, Y., and M. Tokuda, Detection of nonlinear waves and their contribution to ocean wave spectra, I, Theoretical consideration, *J. Oceanogr.*, 51, 385–406, 1995a.
- Hisaki, Y., and M. Tokuda, Detection of nonlinear waves and their contribution to ocean wave spectra, II, Observation, *J. Oceanogr.*, 51, 407–419, 1995b.
- Holden, G. J., and L. R. Wyatt, Extraction of sea state in shallow water using HF radar, *IEE Proc. F*, 139, 175–181, 1992.
- Howell, R., and J. Walsh, Measurement of ocean wave spectra using narrow-beam HF radar, *IEEE J. Oceanic Eng.*, 18, 296–305, 1993.
- Kahma, K. K., and C. J. Calkoen, Reconciling discrep-

- ancies in the observed growth of wind-generated waves, *J. Phys. Oceanogr.*, 22, 1389–1405, 1992.
- Lipa, B. J., Derivation of directional ocean-wave spectra by integral inversion of second-order radar echoes, *Radio Sci.*, 12, 425–434, 1977.
- Lipa, B. J., Inversion of second-order radar echoes from the sea, *J. Geophys. Res.*, 83, 959–962, 1978.
- Lipa, B. J., and D. E. Barrick, Analysis methods for narrow-beam high-frequency radar sea echo, *Tech. Rep. ERL 420-WPL 56*, Natl. Oceanic and Atmos. Admin., Boulder, Colo., 1982.
- Lipa, B. J., and D. E. Barrick, Extraction of sea state from HF radar sea echo: Mathematical theory and modeling, *Radio Sci.*, 21, 81–100, 1986.
- Mitsuyasu, A., F. Tasai, T. Suhara, S. Mizuno, M. Ohkusu, T. Honda, and K. Rikiishi, Observations of the directional spectrum of ocean waves using a cloverleaf buoy, *J. Phys. Oceanogr.*, 5, 750–760, 1975.
- Shanno, D. F., Conjugate gradient methods with inexact searches, *Math. Oper. Res.*, 3, 244–256, 1978.
- Twomey, S., On the numerical solution of Fredholm integral equations of the first kind by the inversion of the linear system produced by quadrature, *J. Assoc. Comput. Mach.*, 10, 97–101, 1963.
- Weber, B. L., and D. E. Barrick, On the nonlinear theory for gravity waves on the ocean's surface, I, Deviations, *J. Phys. Oceanogr.*, 7, 3–10, 1977.
- Wyatt, L. R., A relaxation method for integral inversion applied to HF radar measurement of the ocean wave directional spectra, *Int. J. Remote Sens.*, 11, 1481–1494, 1990.
- Wyatt, L. R., and G. J. Holden, Developments in ocean wave measurement by HF radar, *IEE Proc. F*, 139, 170–174, 1992.
-
- Y. Hisaki, Communications Research Laboratory, Okinawa Radio Laboratory, 829-3 Aza-Kuba, Daigusukubaru, Nakagusuku-son, Nakagami-gun, Okinawa 901-24, Japan. (e-mail: hisaki@crl.go.jp)

(Received January 24, 1995; revised June 28, 1995; accepted August 10, 1995.)